

Plaquette order and deconfined quantum critical point in the spin-1 bilinear-biquadratic Heisenberg model on the honeycomb lattice

H. H. Zhao,¹ Cenke Xu,² Q. N. Chen,³ Z. C. Wei,¹ M. P. Qin,¹ G. M. Zhang,^{4,*} and T. Xiang^{1,3,†}

¹*Institute of Physics, Chinese Academy of Sciences, Beijing 100190, China*

²*Department of Physics, University of California, Santa Barbara, California 93106, USA*

³*Institute of Theoretical Physics, Chinese Academy of Sciences, P.O. Box 2735, Beijing 100190, China*

⁴*State Key Laboratory of Low-Dimensional Quantum Physics and Department of Physics, Tsinghua University, Beijing 100084, China*

(Received 21 February 2012; published 9 April 2012)

We have precisely determined the ground state phase diagram of the quantum spin-1 bilinear-biquadratic Heisenberg model on the honeycomb lattice using the tensor renormalization group method. We find that the ferromagnetic, ferroquadrupolar, and a large part of the antiferromagnetic phases are stable against quantum fluctuations. However, around the phase where the ground state is antiferroquadrupolar ordered in the classical limit, quantum fluctuations suppress completely all magnetic orders, leading to a plaquette order phase which breaks the lattice symmetry but preserves the spin SU(2) symmetry. On the evidence of our numerical results, the quantum phase transition between the antiferromagnetic phase and the plaquette phase is found to be either a direct second order or a very weak first order transition.

DOI: [10.1103/PhysRevB.85.134416](https://doi.org/10.1103/PhysRevB.85.134416)

PACS number(s): 75.10.Kt, 75.10.Jm, 75.40.Mg

I. INTRODUCTION

In a quantum spin system, the spin order of the classical ground state can be melted by a quantum fluctuation at zero temperature,¹ and the resulting so-called quantum spin liquid has been suggested as a possible parent state of high temperature superconductivity upon electron or hole doping.² The quantum fluctuation is usually enhanced with a small spin, low dimensionality, and geometric frustration. Indeed, so far almost all the candidates of a quantum spin liquid discovered or proposed are effective spin-1/2 systems with or without charge fluctuations on a triangular lattice,^{3–7} on a Kagome lattice,^{8–12} or on a honeycomb lattice.^{13–17} Besides the exotic quantum spin liquid phases, strong quantum fluctuations in spin-1/2 systems can also lead to highly unconventional quantum critical points. For example, it has been proposed that a generic direct second order quantum phase transition between a magnetic ordered phase and a paramagnetic phase with broken lattice symmetry can exist in spin-1/2 quantum magnets.^{18,19} Such a transition is forbidden by the classic Landau-Ginzburg-Wilson-Fisher paradigm, and is called the deconfined quantum critical point, as it is described by fractionalized quantities instead of physical order parameters. In the last few years this theoretical proposal has gained strong numerical evidence by quantum Monte Carlo simulation on spin-1/2 models with both nearest neighbor Heisenberg coupling and four-spin interactions.^{20–22}

In this paper we will address the question: Can quantum fluctuation lead to such exotic phases and phase transitions in systems with larger spins in two dimensions without geometric frustration? Theoretically, this question is highly nontrivial as the Affleck-Kennedy-Lieb-Tasaki type of valence bond state (VBS) only exists for spin-1 systems in one dimension. Recent experiments on the spin-1 magnet Ba₃NiSb₂O₉ suggested that a highly nontrivial quantum disordered ground state of a two dimensional spin-1 system is indeed possible.²³

By using the state of the art tensor renormalization group method,^{24–26} we present strong numerical evidences for the quantum fluctuation driven exotic physics in the spin-1

bilinear-biquadratic Heisenberg model on the honeycomb lattice. An interesting but surprising result we find is that all dipole and quadruple magnetic orders vanish in a phase where the ground state is staggered quadrupolar ordered in the classical limit; instead the system develops a translation symmetry breaking plaquette order. Moreover, we demonstrate that the transition between the plaquette and antiferromagnetic (AF) order is either a direct second order transition or a very weak first order transition. If it is indeed a direct second order transition, then it is most likely a deconfined quantum critical point, which is the first example of a deconfined quantum critical point in a spin-1 system.

The spin-1 bilinear-biquadratic Heisenberg model reads

$$H = \sum_{(i,j)} [(\cos \theta) \mathbf{S}_i \cdot \mathbf{S}_j + (\sin \theta) (\mathbf{S}_i \cdot \mathbf{S}_j)^2]. \quad (1)$$

The honeycomb lattice has the smallest coordination number in two dimensions, and the effect of a quantum fluctuation is the strongest. This model contains a number of special points. The point $\theta = 0$ is the conventional SU(2) AF Heisenberg model. When $\theta = \pi/4$, $5\pi/4$, or $\pm\pi/2$, the Hamiltonian is SU(3) invariant, possessing a symmetry higher than the spin SU(2) symmetry. At $\theta_{\pm} = \pm \arctan 2$, the Hamiltonian can be expressed purely using the quadrupolar tensor operator

$$\mathbf{Q}_i = \begin{pmatrix} S_{ix}^2 - S_{iy}^2 \\ \sqrt{3} S_{iz}^2 - 2/\sqrt{3} \\ S_{ix} S_{iy} + S_{iy} S_{ix} \\ S_{iy} S_{iz} + S_{iz} S_{iy} \\ S_{ix} S_{iz} + S_{iz} S_{ix} \end{pmatrix}, \quad (2)$$

as

$$H = \sum_{(i,j)} \left(\frac{\sin \theta_{\pm}}{2} \mathbf{Q}_i \cdot \mathbf{Q}_j + \frac{4}{3} \sin \theta_{\pm} \right). \quad (3)$$

Like the ferromagnetic (FM) spin operator, the uniform quadrupolar operator, $\mathbf{Q} = \sum_i \mathbf{Q}_i$, commutes with this

Hamiltonian. However, the staggered quadruple operator, $\mathbf{Q}_s = \sum_i (-)^i \mathbf{Q}_i$, does not commute with the Hamiltonian.

The two terms in Eq. (1) introduce competition between different kinds of magnetic orders. The first term favors the conventional ferromagnetic or antiferromagnetic order, while the second term favors a ferro- or antiferroquadrupolar order. This competition causes a strong quantum fluctuation, especially in the regime $\sin\theta > 0$, where the Marshall sign rule is not applicable to the ground state wave function and the quantum Monte Carlo suffers the minus-sign problem.

Aspects of the spin-1 bilinear-biquadratic model have been explored previously in the literature. In one dimension, the ground state phase diagram has been characterized by a numerical density matrix renormalization group method. For $-\pi/4 < \theta < \pi/4$, the model gives rise to the Haldane spin gapped phase, while the ground state for $\pi/4 < \theta < \pi/2$ corresponds to a quantum critical phase with power-law spin and quadrupolar correlations.^{27,28}

In two dimensions, the ground state phase diagram has not been firmly established. In the classical limit, this model possesses four phases,^{29,30} as depicted by the inner circle of Fig. 1. In the lower half plane of θ , the quantum Monte Carlo simulation³¹ and other calculations¹⁵ confirmed the classical phase diagram on square or triangular lattices. In the upper half plane of θ , there is no quantum Monte Carlo study on this model due to the minus-sign problem. Other calculations based on mean field theory and exact diagonalization showed that the phase $\pi/4 < \theta < \pi/2$ is antiferroquadrupolar ordered on the triangular or square lattice.³²

II. METHODS

The tensor renormalization group method recently developed is an accurate numerical method for studying the ground

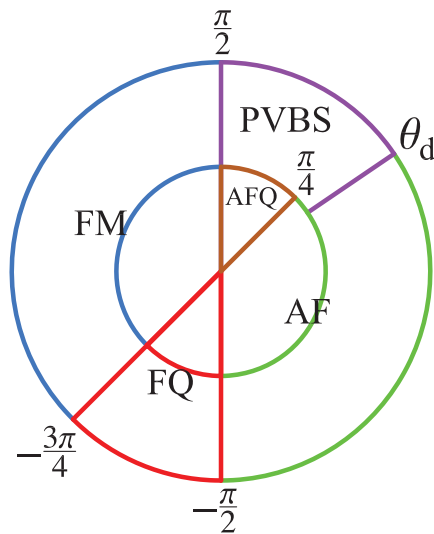


FIG. 1. (Color online) The ground state phase diagram of the spin-1 bilinear-biquadratic Heisenberg model on the honeycomb lattice. The inner circle is the phase diagram in the classical limit, while the outer circle is for the corresponding quantum spin model. FM, AF, FQ, AFQ, and PVBS stand for ferromagnetic, antiferromagnetic, ferroquadrupolar, antiferroquadrupolar, and plaquette valence bond solid phases, respectively. $\theta_d \approx 0.19\pi$.

state of quantum lattice models in two dimensions.^{24–26} It does not have the minus-sign problem encountered in the quantum Monte Carlo simulation and can be used to study the phase diagram in the whole parameter space. We assume that the ground state is described by the following tensor-product wave function

$$|\Psi\rangle = \text{Tr} \prod_{\{i\}} A_{x_i y_i z_i}^i [m_i], \quad (4)$$

where m_i is the eigenvalue of spin operator S_i^z . $A_{x_i y_i z_i}^i [m_i]$ are the third-order tensors defined on the six sublattices, as shown in Fig. 2. The trace is to sum over all spin configurations and all virtual bond variables. This wave function satisfies the area law of entanglement entropy. It is an accurate representation of the ground state wave function. Its accuracy is determined by the bond dimension D . It approaches the exact result in the limit $D \rightarrow \infty$.

The ground state wave function, or the local tensors A^i , is determined by applying the projection operator $\exp(-\tau H)$ to an arbitrary initial state $|\Psi\rangle$ iteratively until it is converged. Since this model only contains nearest neighbor interactions, $\exp(-\tau H)$ can be divided into a sequence of local two-site operators approximately by the Trotter-Suzuki decomposition for a sufficiently small τ . We apply the first order Trotter-Suzuki decomposition here. In our calculation, we start the projection with a relatively large $\tau = 0.2$ and then reduce it gradually to 10^{-4} until the wave function is converged. In order to find the true ground state and not being trapped in a local minimum, we start the projection from a variety of possible magnetically ordered states or valence bond solid states. We choose the converged state which has the lowest energy as the ground state wave function. A detailed introduction to this method can be found from Refs. 24,25. This method is a fast and accurate way to get the ground state wave function.

After obtaining the ground state wave function $|\Psi\rangle$, we can evaluate the expectation value of physical variable O :

$$\langle O \rangle = \frac{\langle \Psi | O | \Psi \rangle}{\langle \Psi | \Psi \rangle}. \quad (5)$$

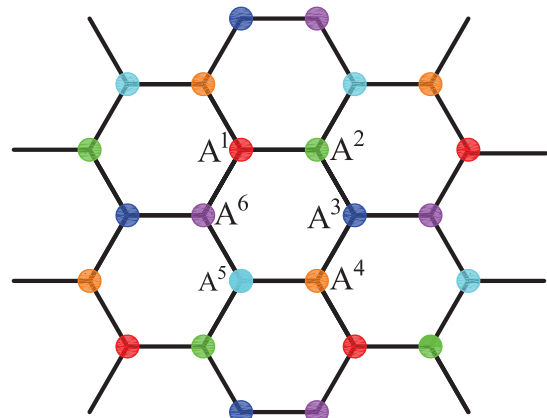


FIG. 2. (Color online) Diagrammatic representation of the tensor-network wave function on the honeycomb lattice. Tensor A^i defined on each lattice site contains three virtual bond indices and one physical index.

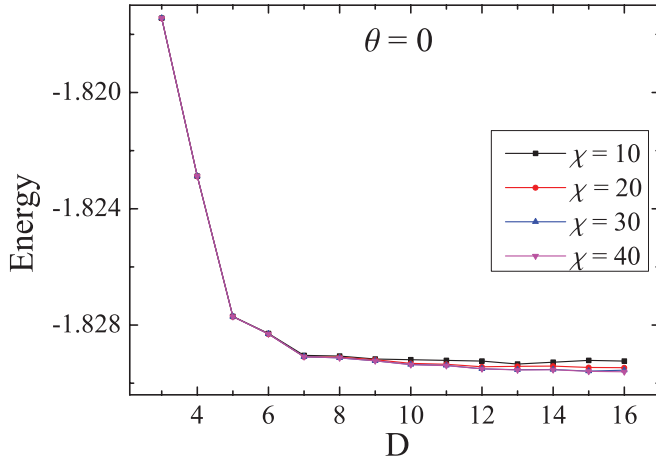


FIG. 3. (Color online) The ground state energy density as a function of D with different values of χ at $\theta = 0$. The curves of $\chi = 30$ and $\chi = 40$ are almost on top of each other.

By contracting the physical indices, both $\langle \Psi | O | \Psi \rangle$ and $\langle \Psi | \Psi \rangle$ can be also expressed as a tensor network. The contraction of tensors is achieved by computing the dominant eigenvector of the corresponding one dimensional transfer matrix using the infinite time-evolving block decimation (iTEBD) method²⁶ beyond unitary evolution. The iTEBD is also an iterative projection method and the truncation error does not accumulate during the iteration. The largest eigenvector of the transfer matrix is represented by a matrix product state with bond dimension χ , which determines the accuracy of the expectation values.

In our calculations, we found that the ground state energy is converged when the bond dimension $D \geq 12$, while the expectation values of physical variables become stable when the parameter $\chi \geq 30$ (see Fig. 3). Thus, we choose $D = 12$ and $\chi = 30$ throughout the calculations.

III. RESULTS

The ground state energy shows that the most part of the quantum phase diagram matches with the classical phase diagram. Figure 4 displays the θ dependence of the ground state energy and Fig. 5 displays its first and second derivatives. The first derivative is calculated with Hellmann-Feynman theorem, which is more accurate than numerical differentiation from the ground state energy. We find that there are four phase transitions, located at $\theta = -3\pi/4$, $\pm\pi/2$, and $\theta_d \approx 0.19\pi$, respectively. Among them, $\theta = -3\pi/4$ and $\pm\pi/2$ are first order transitions. The transition at θ_d is a second order one. This transition point is shifted below the classical value $\theta = \pi/4$, which will be discussed later on.

To clarify the phase diagram, we calculate various order parameters, i.e., the magnetization

$$M^z = \sum_i \langle S_{iz} \rangle, \quad (6)$$

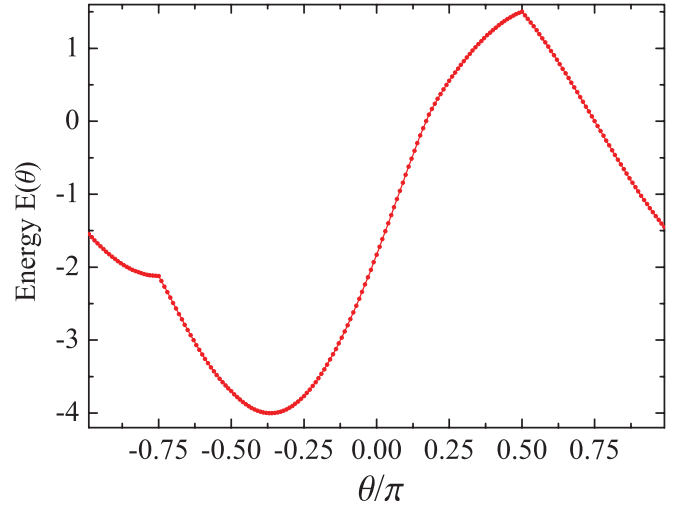


FIG. 4. (Color online) The ground state energy density as a function of θ .

the staggered magnetization

$$M_s^z = \sum_i (-)^i \langle S_{iz} \rangle, \quad (7)$$

the ferroquadrupolar moment

$$Q^{zz} = \sum_i \langle S_{iz}^2 \rangle - 2/3, \quad (8)$$

and the antiferroquadrupolar moment

$$Q_s^{zz} = \sum_i (-)^i \langle S_{iz}^2 \rangle, \quad (9)$$

in the four phases, respectively. Figure 6 shows the θ dependence of M^z and M_s^z . The ground state is found to have FM long-range order for $\pi/2 < \theta < 5\pi/4$, and AF long-range order for $-\pi/2 < \theta < \theta_d$. In these phases, the quadrupole moment Q^{zz} is finite. In the region $-3\pi/4 < \theta < -\pi/2$, both magnetization and staggered magnetization vanish; however, the quadrupolar moment is finite, as shown in Fig. 7. It

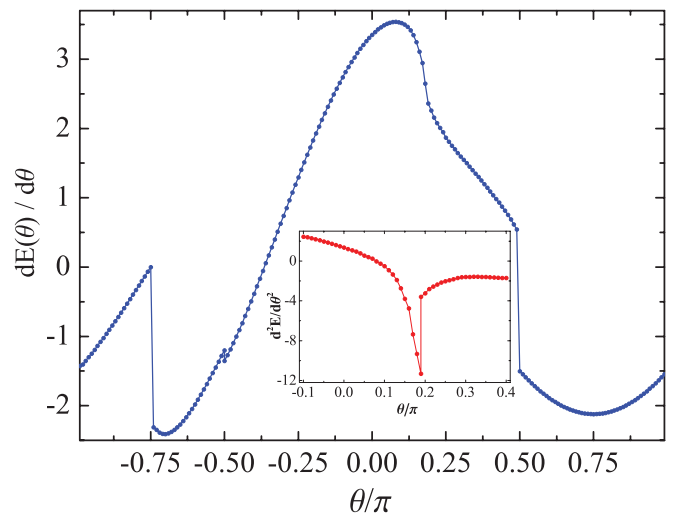


FIG. 5. (Color online) The first and second (the inset) derivatives of the ground state energy with respect to θ .

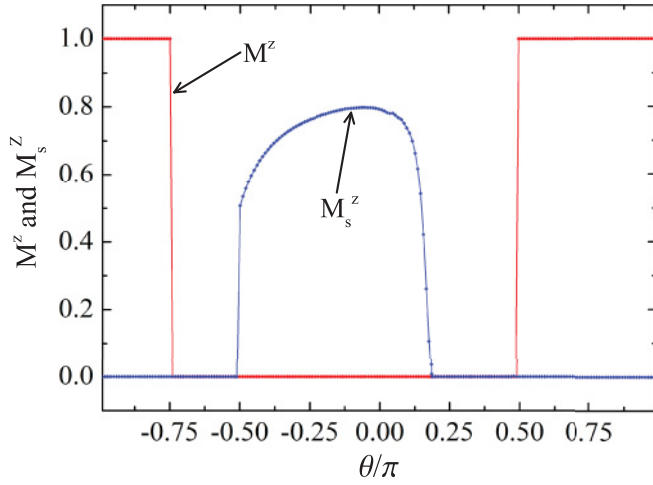


FIG. 6. (Color online) Uniform (red) line and staggered (blue) line represent magnetization per site as a function of θ .

corresponds to a ferroquadrupolar phase, in agreement with both the semiclassical^{29,30} and quantum Monte Carlo³¹ results.

In the staggered magnetization curve a sharp jump shows at $\theta_c = -\pi/2$. This feature was also observed in the quantum Monte Carlo calculation on a square lattice.³¹ But the quadrupolar moment is finite and changes continuously at this point. So a first order phase transition occurs, in consistence with the conclusion drawn from the first derivative of the ground state energy.

As expected, the staggered quadrupolar moment Q_s^{zz} vanishes in the FM, AF, and ferroquadrupolar phases. A surprising result is that this moment also vanishes in the classical staggered quadrupolar phase $\pi/4 < \theta < \pi/2$, i.e., the quantum fluctuation suppresses completely the staggered quadrupolar order, which is different from the previous studies on the triangular or square lattices.³² More interestingly, the critical point has been shifted by the quantum fluctuation from $\pi/4$ to about 0.19π , which excludes the SU(3) AF Heisenberg spin-1 model from any long-range magnetic order.

To further characterize the phase for $\theta_d < \theta < \pi/2$, we have performed a thorough exploration of three possible VBS

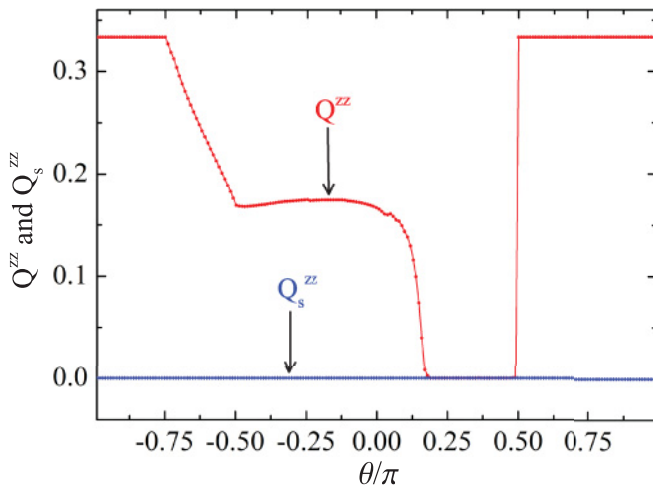


FIG. 7. (Color online) Uniform (red) line and staggered (blue) line represent spin quadrupole moment per site as a function of θ .

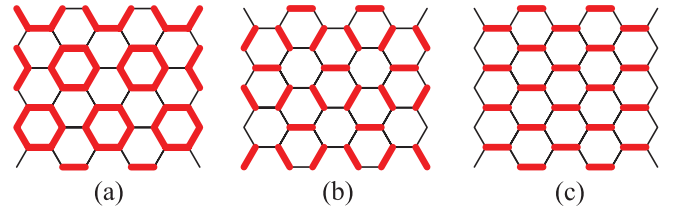


FIG. 8. (Color online) Pictorial representation of three possible VBS patterns considered in the calculation: (a) plaquette, (b) columnar, and (c) staggered. The red thicker bonds represent stronger correlation while the black thinner bonds represent weaker correlation.

patterns (Fig. 8) on the honeycomb lattice. It has been checked that whatever VBS patterns we start with, it always converges into the plaquette order phase [Fig. 8(a)] under renormalization group flow. Hence the ground state energy of the plaquette VBS phase is the lowest. This plaquette order phase explicitly breaks the lattice translation symmetry, but not the spin SU(2) symmetry. A naive picture of this plaquette order is that, in order to minimize the ground state energy, the spins on one-third of the minimal hexagons of the honeycomb lattice form the VBS phase, like the Haldane gapped phase in one dimension.

In order to detect the plaquette order, we calculate the plaquette order parameter defined as

$$P = \frac{\sum_{\langle i,j \rangle \in \text{red}} \langle \mathbf{S}_i \cdot \mathbf{S}_j \rangle}{2 \sum_{\langle i,j \rangle \in \text{black}} \langle \mathbf{S}_i \cdot \mathbf{S}_j \rangle} - 1, \quad (10)$$

where $\langle i,j \rangle \in \text{red}$ (black) means the two nearest neighbor spins connected by red (black) bonds of Fig. 8(a). Figure 9 shows the θ dependence of the plaquette order parameters. Both the plaquette and AF orders vanish simultaneously and continuously at the critical point θ_d . This observation suggests that this plaquette-AF transition is in fact a second order transition, in consistence with the conclusion drawn from the first and second derivatives of the ground state energy with respect to θ in Fig. 5. But we are still unable to rule out the

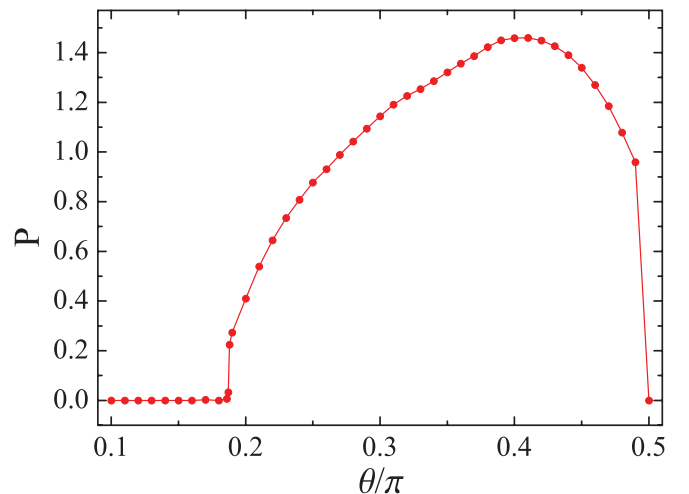


FIG. 9. (Color online) The plaquette order parameter as a function of θ .

possibility of a very weak first order transition, partly due to the finite bond dimension D .

Moreover, around the transition point between antiferromagnetic and plaquette valence bond solid phases, we have evaluated the ground state wave function using the cluster update approach proposed by Wang *et al.*³³ The cluster update considers long-range entanglement by computing a larger block size. The accuracy of the computation near a second order phase transition can be improved by using a relatively small cluster size (six sites).

IV. DISCUSSION AND CONCLUSION

A second order transition between AF and VBS order was originally predicted theoretically as the deconfined quantum critical point. This theory is based on the observation that the topological defect (Skyrmion) of the AF order parameter carries a finite lattice momentum; thus after the AF order is suppressed by the Skyrmion proliferation, the system automatically enters the VBS order. The previous studies on deconfined criticality were focused on spin-1/2 systems only, and this theory has gained strong numerical evidence from quantum Monte Carlo simulation on a spin-1/2 model on the square lattice with both two-body and four-body interactions.^{20–22} Our present result actually gives rise to a possible deconfined quantum critical point in the spin-1 systems. Using the techniques in Refs. 34,35, we can show that for spin-1 systems on the honeycomb lattice the momenta carried by the Skyrmion will precisely lead to the plaquette order pattern after the Skyrmion proliferation.

In fact, another columnar VBS order [Fig. 8(b)] has the same symmetry as the plaquette order, which in principle can also be a candidate phase of the Skyrmion condensate. However, in this part of the phase diagram the energy of the

columnar VBS order is higher than the plaquette order. One can see this by noting that the SU(3) invariant point is in this plaquette phase, and the plaquette phase can be adiabatically connected to a SU(3) singlet phase, while the VBS order in Fig. 8(b) cannot. Thus we conclude that the plaquette order is energetically more favorable than the columnar VBS order close to the SU(3) point.

Due to the critical point between AF and plaquette order at θ_d , our numerical result also implies that the ground state of the SU(3) AF Heisenberg model on the honeycomb lattice has a plaquette order. This result concurs with the recent studies on the SU(N) Heisenberg model,³⁶ which suggested that the SU(N) spins tend to form block singlets that are commensurate with the lattice.

To summarize, the ground state phase diagram of the quantum spin-1 bilinear-biquadratic Heisenberg model on a honeycomb lattice has been determined precisely. Besides the ferromagnetic, antiferromagnetic, and ferroquadrupolar phases, a plaquette order phase is found in the region of $\theta_d < \theta < \pi/2$, where the classical AF or staggered quadrupolar order is completely suppressed by quantum fluctuations. The quantum phase transition between AF and the plaquette order phase is found to be either a direct second order or a very weak first order transition. This is a possible candidate of a deconfined quantum critical point in a quantum spin-1 system. Further investigation on the critical properties around this point is desired.

ACKNOWLEDGMENTS

We would like to thank Ling Wang for stimulating discussions. This work is supported by NSFC and the grants of the National Program for Basic Research of MOST of China. C.X. is supported by the Sloan Research Fellowship.

*gmzhang@tsinghua.edu.cn

†txiang@iphy.ac.cn

¹P. W. Anderson, *Mater. Res. Bull.* **8**, 153 (1973).

²P. W. Anderson, *Science* **235**, 1196 (1987).

³S. Yamashita *et al.*, *Nat. Phys.* **4**, 459 (2008).

⁴M. Yamashita *et al.*, *Nat. Phys.* **5**, 44 (2009).

⁵M. Yamashita *et al.*, *Science* **328**, 1246 (2010).

⁶T. Itou *et al.*, *Nat. Phys.* **6**, 673 (2010).

⁷G. Misguich, B. Bernu, C. Lhuillier, and C. Waldtmann, *Phys. Rev. Lett.* **81**, 1098 (1998).

⁸J. S. Helton *et al.*, *Phys. Rev. Lett.* **98**, 107204 (2007).

⁹S. H. Lee *et al.*, *Nat. Mater.* **6**, 853 (2007).

¹⁰Y. Okamoto *et al.*, *J. Phys. Soc. Jpn.* **78**, 033701 (2009).

¹¹Z. Hiroi *et al.*, *J. Phys. Soc. Jpn.* **70**, 3377 (2001).

¹²S. Yan, D. A. Huse, and S. R. White, *Science* **332**, 1173 (2011).

¹³F. Wang, *Phys. Rev. B* **82**, 024419 (2010).

¹⁴B. K. Clark, D. A. Abanin, and S. L. Sondhi, *Phys. Rev. Lett.* **107**, 087204 (2011).

¹⁵A. F. Albuquerque, D. Schwandt, B. Hetenyi, S. Capponi, M. Mambrini, and A. M. Lauchli, *Phys. Rev. B* **84**, 024406 (2011).

¹⁶J. Reuther, D. A. Abanin, and R. Thomale, *Phys. Rev. B* **84**, 014417 (2011).

¹⁷Z. Y. Meng, T. C. Lang, S. Wessel, F. F. Assaad, and A. Muramatsu, *Nature (London)* **464**, 847 (2010).

¹⁸T. Senthil, A. Vishwanath, L. Balents, S. Sachdev, and M. P. A. Fisher, *Science* **303**, 1490 (2004).

¹⁹T. Senthil, L. Balents, S. Sachdev, A. Vishwanath, and M. P. A. Fisher, *Phys. Rev. B* **70**, 144407 (2004).

²⁰A. W. Sandvik, *Phys. Rev. Lett.* **98**, 227202 (2007).

²¹R. G. Melko and R. K. Kaul, *Phys. Rev. Lett.* **100**, 017203 (2008).

²²J. Lou, A. W. Sandvik, and N. Kawashima, *Phys. Rev. B* **80**, 180414(R) (2009).

²³J. G. Cheng, G. Li, L. Balicas, J. S. Zhou, J. B. Goodenough, Cenke Xu, and H. D. Zhou, *Phys. Rev. Lett.* **107**, 197204 (2011).

²⁴H. C. Jiang, Z. Y. Weng, and T. Xiang, *Phys. Rev. Lett.* **101**, 090603 (2008); Z. Y. Xie, H. C. Jiang, Q. N. Chen, Z. Y. Weng, and T. Xiang, *ibid.* **103**, 160601 (2009).

²⁵H. H. Zhao, Z. Y. Xie, Q. N. Chen, Z. C. Wei, J. W. Cai, and T. Xiang, *Phys. Rev. B* **81**, 174411 (2010).

²⁶G. Vidal, *Phys. Rev. Lett.* **98**, 070201 (2007); J. Jordan, R. Orús, G. Vidal, F. Verstraete, and J. I. Cirac, *ibid.* **101**, 250602 (2008).

- ²⁷G. Fath and J. Solyom, *Phys. Rev. B* **44**, 11836 (1991).
- ²⁸T. Xiang and G. A. Gehring, *Phys. Rev. B* **48**, 303 (1993).
- ²⁹H. H. Chen and P. M. Levy, *Phys. Rev. B* **7**, 4267 (1973).
- ³⁰N. Papanicolaou, *Nucl. Phys. B* **305**, 367 (1988).
- ³¹K. Harada and N. Kawashima, *J. Phys. Soc. Jpn.* **70**, 13 (2001); *Phys. Rev. B* **65**, 052403 (2002).
- ³²A. Lauchli, F. Mila, and K. Penc, *Phys. Rev. Lett.* **97**, 087205 (2006); T. A. Toth, A. M. Lauchli, F. Mila, and K. Penc, *ibid.* **105**, 265301 (2010).
- ³³L. Wang and F. Verstraete, e-print [arXiv:1110.4362](https://arxiv.org/abs/1110.4362).
- ³⁴F. D. M. Haldane, *Phys. Rev. Lett.* **61**, 1029 (1988).
- ³⁵N. Read and S. Sachdev, *Phys. Rev. B* **42**, 4568 (1990).
- ³⁶M. Hermele, V. Gurarie, and A. M. Rey, *Phys. Rev. Lett.* **103**, 135301 (2009).